



Article

Low symmetric sub-wavelength array enhanced lensless polarization-sensitivity photodetector of germanium selenium

Ziqi Zhou^{a,b,c}, Tao Shen^{a,c}, Pan Wang^{a,c}, Quanlin Guo^b, Qinghe Wang^b, Chenjun Ma^b, Kaiyao Xin^{a,c}, Kai Zhao^{a,c}, Yali Yu^{a,c}, Biao Qin^b, Yue-Yang Liu^{a,c}, Juehan Yang^{a,c}, Hao Hong^b, Kaihui Liu^b, Can Liu^{d,*}, Hui-Xiong Deng^{a,c,*}, Zhongming Wei^{a,c,*}

^a State Key Laboratory of Superlattices and Microstructures, Institute of Semiconductors, Chinese Academy of Sciences, Beijing 100083, China

^b State Key Laboratory for Mesoscopic Physics, Frontiers Science Centre for Nano-optoelectronics, School of Physics, Peking University, Beijing 100871, China

^c Center of Materials Science and Optoelectronics Engineering, University of Chinese Academy of Sciences, Beijing 100049, China

^d Department of Physics, Renmin University of China, Beijing 100872, China

ARTICLE INFO

Article history:

Received 27 October 2022
Received in revised form 17 December 2022
Accepted 10 January 2023
Available online 10 January 2023

Keywords:

Germanium selenium (GeSe)
Polarization-sensitive photodetectors
Sub-wavelength array
Anisotropy ratio

ABSTRACT

Polarization-sensitive photodetectors, with the ability of identifying the texture-, stress-, and roughness-induced light polarization state variation, possess unique advantages in the fields of national security, medical diagnosis, and aerospace. The utilization of in-plane anisotropic two-dimensional (2D) materials has led the polarization photodetector into a polarizer-free regime, and facilitated the miniaturization of optoelectronic device integration. However, the insufficient polarization ratio (usually less than 10) restricts the detection resolution of polarized signals. Here, we designed a sub-wavelength array (SWA) structure of 2D germanium selenium (GeSe) to further improve its anisotropic sensitivity, which boosts the polarized photocurrent ratio from 1.6 to 18. This enhancement comes from the combination of nano-scale arrays with atomic-scale lattice arrangement at the low-symmetric direction, while the polarization-sensitive photoresponse along the high-symmetric direction is strongly suppressed due to the SWA-caused depolarization effect. Our mechanism study revealed that the SWA can improve the asymmetry of charge distribution, attenuate the matrix element in zigzag direction, and the localized surface plasma, which elevates the photo absorption and photoelectric transition probability along the arm-chair direction, therefore accounts for the enhanced polarization sensitivity. In addition, the photodetector based on GeSe SWA exhibited a broad power range of 40 dB at a near-infrared wavelength of 808 nm and the ability of weak-light detection under 0.1 LUX of white light (two orders of magnitude smaller than pristine 2D GeSe). This work provides a feasible guideline to improve the polarization sensitivity of 2D materials, and will greatly benefit the development of polarized imaging sensors.

© 2023 Science China Press. Published by Elsevier B.V. and Science China Press. All rights reserved.

1. Introduction

Polarization of light, carrying multi-dimensional information of polarization degree, phase shift, and Jones vector, is critical in applications of remote sensing, visual imaging, and navigation [1–3]. To effectively detect the tremendous polarization states, polarization-sensitive photodetectors have been developed since the 1980s [4–9]. And its main development course went through three periods, i.e., the time division stage (polarization states are

detected by stepwise rotating polarizer) [10], the space division stage (polarization states are detected by splitting light into four separate detectors) [11], and the focal plane polarimeter stage (polarization states are detected by four directional micro-metal polarizers integrated on detectors) [12,13]. However, the commercially-used polarization-sensitive photodetectors of focal-plane polarimeters still suffer from fewer Stokes parameters, pixel cross-talk, and are unable to detect wavelengths smaller than the grating size of the polarimeter [14]. In contrast, the recently developed polarizer-free photodetector shows the ability of full Stokes parameter and broad-spectrum detection, and can naturally get rid of the pixel cross-talk issue, making it promising for next-generation polarization-sensitive photodetectors with high resolution and integration.

* Corresponding authors.

E-mail addresses: canliu@ruc.edu.cn (C. Liu), hxdeng@semi.ac.cn (H.-X. Deng), zmwei@semi.ac.cn (Z. Wei).

Two-dimensional (2D) materials have developed rapidly in the field of photodetector for their high responsivity, low dark current, and fast photoresponse [15–18]. Among them, in-plane anisotropic 2D materials, with their atomically-thin thickness, natural in-plane linear dichroism and anisotropic photoresponse, have been demonstrated to be the most ideal candidates for the polarizer-free imaging sensor [19–30]. The optimal in-plane anisotropic material, black phosphorus (BP), exhibited a polarization ratio of 8.9 in the near-infrared (NIR) range, but still struggled from the structure instability under ambient conditions [24,31–34]. Nevertheless, other stable 2D anisotropic materials, e.g., BAs, GeS₂, GeS, SnS, and ReS₂, exhibited inadequate polarization ratio (usually less than 10) [35–42]. Hence, in-plane anisotropic 2D materials with high anisotropic photocurrent and environmental resistance are highly desired for lightweight polarization-sensitive photodetectors.

GeSe, the isolectronic group of BP, belonging to the orthorhombic crystal system (*Pcmm-D_{2h}*) [43], was widely applied to NIR polarization-sensitive photodetectors due to its narrow band gap (1.1 eV), high linear dichroism ratio (3.02) and structure stability [44,45]. However, its representative anisotropic ratio of 3.4 (less than the standard value of 10 for clear polarization imaging [46]) was inadequate to obtain clear information of the target [47]. Various efforts of external systems such as constructing heterostructures [48,49], homojunction [50], and coupling with amplifying circuit [51–53] have been made to enhance its polarization sensitivity. However, these external systems have some inherent drawbacks, like complex design, limited miniaturization, and high cost. Therefore, a universal method is highly expected to magnify the intrinsic anisotropic property of GeSe, which is the ultimate purpose for the high resolution of polarization-sensitive photodetectors.

Herein, we designed the sub-wavelength array (SWA) structure on GeSe to modulate its intrinsic polarization-sensitive photocurrents. The combination of the nano-scale arrays and the atomic-scale lattice arrangement could further improve the anisotropy of GeSe. And the selection of an aligned array along the low-symmetric axis could introduce the depolarization effect, manifesting the suppression of photoresponse in the high-symmetric axis. This improved polarization sensitivity comes from the enhanced photon absorption and photoelectric transition probability along the low-symmetric direction, which further accounts for the high polarization ratio and high-resolution detection of GeSe based photodetector.

2. Experimental

2.1. Growth of GeSe single crystal

In the growth, the precursors adopt commercially available Ge powder (99.99%, Aladdin), Se powder (99.99%, Aladdin) and iodine (99%, Alpha). All of the reaction precursors (Ge powder and Se powder with the equal molar mass) and catalyst (the iodine of 0.05 g) were securely sealed in the quartz tube (with a length of 20 cm) with high vacuum, and then, the quartz tube is loaded into two-zone high temperature tube furnace (2 inch). The chamber of furnace was heated to the optimized growth temperature (700 °C for complete evaporation of precursors and 400 °C for the growth of GeSe), while the growth duration was set as 300–500 h. After growth, the temperature of tube furnace down to 200 °C with a cooling rate of 20 °C/h and then natural cooling down to room temperature. Finally, we can obtain the high quality GeSe bulk crystals (with the size of 0.5–1.0 cm²).

2.2. Fabrication of SWA pattern and photodetector

In the process of device fabrication, the micro/nano processing technology was multiple utilized. After mechanical exfoliating GeSe flake from bulk crystal onto the SiO₂/Si substrate, angle-resolved Raman spectrum was utilized to determine the zigzag and armchair axis of GeSe flake. Afterward, the sub-wavelength pattern was designed along the armchair direction and transferred to the mask of ZEP film (the thickness of 100 nm) by E-beam lithography. Then, the inductively coupled plasma (ICP) with Cl atmosphere was unitized to etch the GeSe flake with the etching ratio of 4 Å/s. After dissolving ZEP by polymethyl formamide solution under 70 °C, the microstructure could be obtained. In the process, the size of microstructure only depended on the size of ZEP mask. The sharp of edge states was confirmed by the cross-sectional annular dark field scanning transmission electron microscopic (ADF-STEM) image (Fig. S6 online).

The electrode pattern of the photodetector was engraved by secondary E-beam lithography (EBL), and the electrode metal of Cr/Au (the thickness of 10 nm/50 nm, the work function of Cr match with that of GeSe) was evaporated by electron-beam evaporation at the high vacuum of $\sim 10^{-7}$ torr (1 Pa $\approx 7.5 \times 10^{-3}$ torr).

2.3. Polarizing microscope measurements

The in-plane anisotropic crystal has a birefringence phenomenon. Therefore, the polarizing microscope is an effective method for detecting the anisotropic sample. Before measurement, the polarization analyzer was adjusted to orthogonal with incident polarized light. We fixed the analyzer and incident light, and rotated the sample in a uniform speed to observe the brightness changes.

2.4. Angle-dependent Raman spectrum and second-harmonic generation (SHG) measurements

Raman spectrum and SHG were measured by Witec commercial equipment with the excitation wavelength of 532 nm (Raman spectrum, the power of ~ 1 mW) and 1064 nm (SHG, the power of 10 to 20 mW). In the angle dependent measurement, the polarization direction of the analyzer is parallel (parallel mode) or vertical (cross mode) to the polarized excitation light.

2.5. Scanning transmission electron microscope (STEM) characterizations

STEM and energy dispersive X-ray spectroscopy (EDS) characters were performed by FEI Titan Themis G2 300 operated at 300 kV for element analysis and characterizing atomic structures of samples.

2.6. Computational details

The first-principle method of projector-augmented wave (PAW) [54,55] based on the frame-work of density functional theory (DFT) [56] in the Vienna *Ab Initio* Simulation Package (VASP) was utilized to perform the electronic and optical properties of GeSe flake and GeSe SWA. To correct the band gap of experimental value, the Heyd-Scuseria-Ernzerhof (HSE) [57] method with the fraction of exact exchange of 0.21 was adopted for the exchange–correlation function. The kinetic energy cut off for the plane wave expansion was set as 65 Ry, and the SG15 Optimized Norm-Conserving Vanderbilt (ONCV) Perdew–Burke–Ernzerhof (PBE) pseudopotentials [58] was utilized. The Brillouin zone was divided into

$9 \times 7 \times 3$ k-mesh for GeSe flake, $9 \times 1 \times 3$ k-mesh for armchair direction of GeSe array, and $1 \times 7 \times 3$ k-mesh for zigzag direction of GeSe array. For array, the line width was set as 3 periods and 5 periods of GeSe unit-cell. To eliminate the interactions between arrays, a large vacuum layer of about 17–22 Å was added around the array boundary (Fig. S11 online). For the lattice relaxation, each atom was fully relaxed under guaranteeing atomic force of less than 0.01 eV/Å. To calculate the optical absorption properties, the random phase approximation (RPA) approach was adopted.

Numerical simulations were processed using the Wave Optics Module of COMSOL Multiphysics software. The light electric field distribution was calculated using the finite element method in COMSOL. For the numerical modelling, the GeSe layer of 50 nm thickness is placed on 300 nm SiO₂ with Si substrate.

3. Results and discussion

3.1. Selection of the sub-wavelength array direction

The atomic arrangement and charge density distribution are crucial for the selection of the array direction. From the top-view charge density mapping of the band edges, GeSe exhibited a series of charge distribution chains along the armchair direction, demonstrating it as the polarization-sensitive direction (Fig. 1b). Therefore, it is expected that arrays fabricated along the armchair direction can enhance the polarization ratio due to the depolarization effect of the one-dimensional GeSe arrays (Fig. 1a and Fig. S1 online).

In our experiment, GeSe single crystal was synthesized by the chemical vapor transport (CVT) method (see Experimental for details), and then exfoliated on the Cu grid to study the crystallinity and crystalline structure (Fig. S2 online). The high-angle annular dark field scanning transmission electron microscope (HAADF-STEM) image showed the perfect rhombic lattice of GeSe crystal, with each light point corresponding to a pair of Ge-Se atoms (Fig. 1c). The selected area electron diffraction (SAED) pattern under the [001] crystal zone axis demonstrated the orthorhombic crystal structure (Fig. 1d). These results definitely

confirm the high quality and anisotropic atom arrangement of GeSe crystal, which can further guide the fabrication of arrays along the low-symmetric armchair direction.

3.2. Fabrication of the sub-wavelength array along the armchair direction

To accurately fabricate the sub-wavelength array along the armchair direction, the angle-resolved Raman spectroscopy was utilized to figure out the atomic arrangement of GeSe crystal, and the polarization anisotropy of SHG susceptibility was utilized to ascertain the symmetry of the GeSe lattice. As shown in Fig. 2b, the normal Raman spectrum of GeSe exhibited three characteristic peaks, i.e., the out-of-plane A_{1g}¹ mode (~88 cm⁻¹), the in-plane B_{2g} (~150 cm⁻¹) and A_{1g}³ (~188 cm⁻¹) mode. Among them, the B_{2g} and A_{1g}³ modes are assigned as the vibrations along the zigzag and armchair direction respectively [42] (Fig. S3 online). Therefore, the maximal intensity of the angle-resolved A_{1g}³ mode is strong evidence in identifying the armchair direction (Fig. 2c), and the corresponding arrays patterned along this direction can be accurately achieved (Fig. 2a and Fig. S4 online). The brightness variation with the rotation angle under the polarization-resolved optical microscope preliminary proved the birefringence effect of the GeSe SWA (Fig. 2d), indicating its anisotropic optical property after patterned.

A pronounced SHG peak was raised since the C_{2v} (mm2) space group of GeSe (Fig. 2e and Fig. S5a online). The highly asymmetric SHG response petals of parallel (*I*_{||}) and perpendicular (*I*_⊥) to the incident polarization show the two-rotation axis of symmetry existed in GeSe lattice proving the high in-plane anisotropy (Fig. 2f and Fig. S5b online). The shape of SHG petals is consistent with the reported theoretical prediction. In addition, sub-wavelength arrays pattern of GeSe maintain two petals along armchair direction in the parallel polarized SHG patterns, which reveal the strong depolarization effect in SWA pattern [43]. All of these results ultimately demonstrate the fabrication accuracy in patterning the GeSe arrays along the armchair direction.

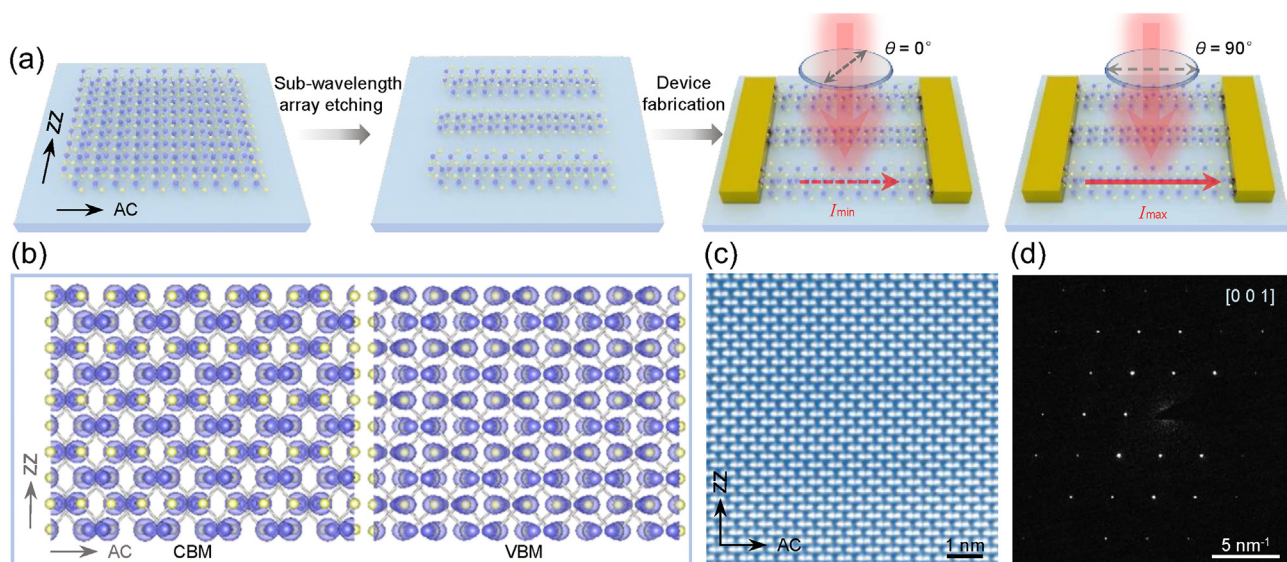


Fig. 1. The sub-wavelength array (SWA) fabrication of GeSe. (a) Schematic of the GeSe SWA photodetector fabrication process, consisting of the array etching along the armchair (AC) direction perpendicular to the zigzag (ZZ) direction and the two-terminal electrodes deposition procedure. The photocurrent reaches its maximum (I_{\max})/minimum (I_{\min}) when the polarized light is parallel/vertical to the armchair direction. (b) The charge density mapping of VBM and CBM states of GeSe, indicating that the charge mainly distributes along the armchair direction. Atomically-resolved STEM image (c) and SAED pattern (d) of GeSe under the crystal axis of [001], demonstrating the high quality of GeSe crystal.

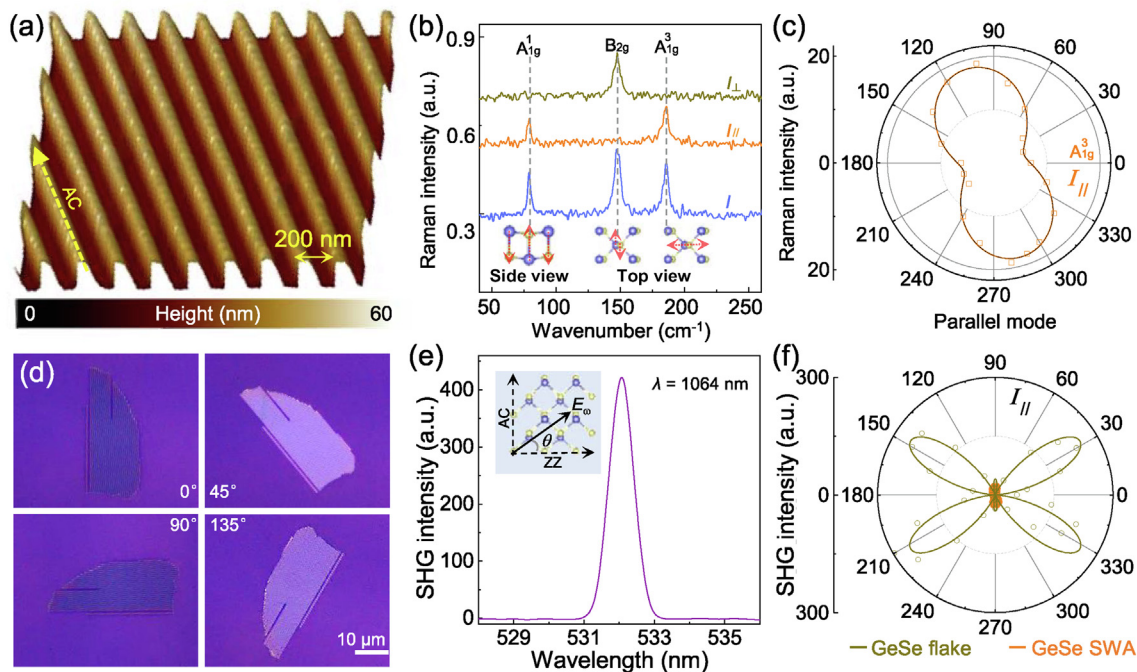


Fig. 2. Identification of the GeSe array patterning orientation. (a) 3D-atomic force microscopic (AFM) image of GeSe SWA patterning along the armchair direction. (b) Polarized Raman spectra detected at the normal mode (I_{\perp} , without the polarization analyzer), parallel mode (I_{\parallel} , the direction of polarization analyzer parallel to polarized angle of excitation laser) and cross mode (I_{\perp} , the direction of polarization analyzer perpendicular to polarized angle of excitation laser), respectively. (c) Angle-resolved Raman intensity pattern of A_{1g}^3 peak, at which the intensity reaches the maximum along the armchair direction of GeSe atomic arrangement. (d) Polarizing microscopic reflection images of GeSe SWA at different angles of incident light polarization. (e) SHG spectrum of GeSe SWA excited by 1064 nm laser. Inset: polarization anisotropy of GeSe SHG susceptibilities, while θ is the rotation angle between incident electric field (E_0) and zigzag direction. (f) Angle-dependent parallel component of SHG from GeSe flake (dark yellow curve) and GeSe SWA of 200 nm period width (orange curve) respectively.

3.3. The optoelectronic properties of GeSe sub-wavelength array photodetector

To study the photoresponse of GeSe SWA, a two-terminal photodetector (Fig. S7 online) based on the optimal GeSe thickness of around 50 nm (Table S1 online) was fabricated by connecting the arrays in parallel and then excited by the 808 nm laser (see Experimental). As shown in Fig. 3b, the photodetector exhibited a high photoresponsivity of 30 A/W, which proved that the GeSe crystal can maintain its excellent photoresponse after the array patterning process. Furthermore, the power-dependent photocurrent curve of GeSe SWA photodetector displayed an excellent dynamic range value of 40 dB (Fig. 3c) within the linear power range of 0.001 to 1 mW/cm², demonstrating the improved detection sensitivity of the SWA-based photodetector. In addition to the ability in detecting the NIR light, the GeSe SWA also showed perfect performance in weak-light detection under 0.1 LUX illumination, and the minimum detection power is two orders of magnitude better than the pristine 2D GeSe-based photodetectors (Fig. 3d).

As for the polarized light detection, the armchair-orientated GeSe SWA indeed possessed better anisotropic photoresponse as we predicted. As shown in Fig. 3e, the polarization ratio (PR) of GeSe array patterned along the armchair direction (PR = 6.7) was significantly increased compared with that of the zigzag ones (PR = 1.1), and the corresponding device image located in Fig. S8 (online). It is worth noting that the weakest photocurrent appeared at 0° (polarized light paralleled to zigzag direction) and the strongest value at 90° (polarized light paralleled to armchair direction) for both the armchair- and zigzag-orientated arrays. Among them, the armchair one showed a significant photocurrent decrease at 0° polarized light due to the depolarization effect along the zigzag direction. Meanwhile, it also displayed a robust increment of

polarization ratio compared with the pristine GeSe flake in the visible to NIR range especially at 400 and 800 nm, and reached a highest value at 808 nm near the band gap edge of GeSe (Fig. 3f).

Besides the array orientation, the intrinsic structure of GeSe arrays (such as the individual array width of W_1 , the repetition period width of W_2 , and the proportion of W_1/W_2 , as shown in the top panel of Fig. 3a) could further modulate the polarization ratio. As shown in Fig. 3g, the photocurrent anisotropy becomes monotonously increasing along with the decreased width of W_2 . And the optimal SWA size of 200 nm period-width reaches the limiting size of the fabricating process (Fig. S9 online). Meanwhile, at a narrow period-width of 200 nm and W_1/W_2 proportion of 25%, an optimal polarization ratio of 18 was obtained, which is an order of magnitude higher than the pristine GeSe photodetectors. The polarization ratio value commendably satisfies the demand of high resolution photodetection (anisotropy ratio >10) (Fig. 3h) under the excitation wavelength of 800 nm, and is significantly improved compared with the typical 2D in-plane anisotropic materials, like SbSSe, GeAs, and BP in the wavelength range of 300–1000 nm.

3.4. Mechanism of the sub-wavelength array induced polarization ratio enhancement

To understand the mechanism of polarization ratio enhancement caused by the SWA pattern, the first-principle calculations were utilized to explore the variation of band structure, matrix elements, and optical adsorption properties in both the GeSe flake and GeSe SWA. In comparison with the band structure of GeSe flake, the quantum restriction effect was observed in GeSe SWA along the zigzag direction (from Γ to Y), which can affect the transition probability of the carrier and the intrinsic optical adsorption (Fig. 4a, d and Fig. S10 online). Specifically, the transition probab-

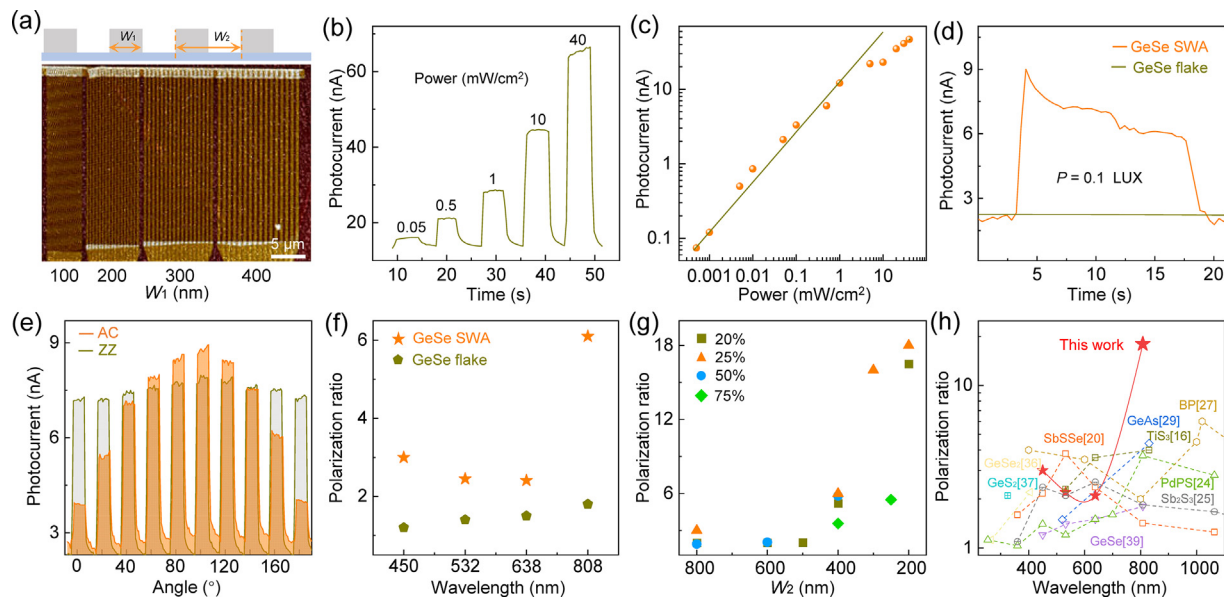


Fig. 3. Photoelectronic characterization of GeSe SWA. (a) The side view schematic of GeSe SWA (top panel). The width of array and the width of repetition period are denoted as W_1 and W_2 respectively. AFM image of GeSe SWA devices with four different array widths (bottom panel). (b) Time evolution of the photocurrent under different power densities of 808 nm laser. (c) Incident-power-dependence photocurrents at 808 nm laser illumination. The linear detection power density is from 0.001 to 1 mW/cm². (d) The white-light illuminated photocurrent of GeSe flake and GeSe SWA under power of 0.1 LUX, displaying the weak-light-detection ability of GeSe SWA. (e) Angle-dependent polarized photocurrent of GeSe SWA photodetector patterned along the armchair and zigzag direction. (f) Comparison of the polarization ratio between the GeSe flake and the GeSe SWA at different excitation wavelength. (g) The polarization ratio of GeSe SWA with different length of W_2 and proportion of W_1/W_2 . (h) Overview of the polarization ratio of series of anisotropic 2D materials previously reported. Our GeSe SWA showed a pronounced increase in polarization ratio.

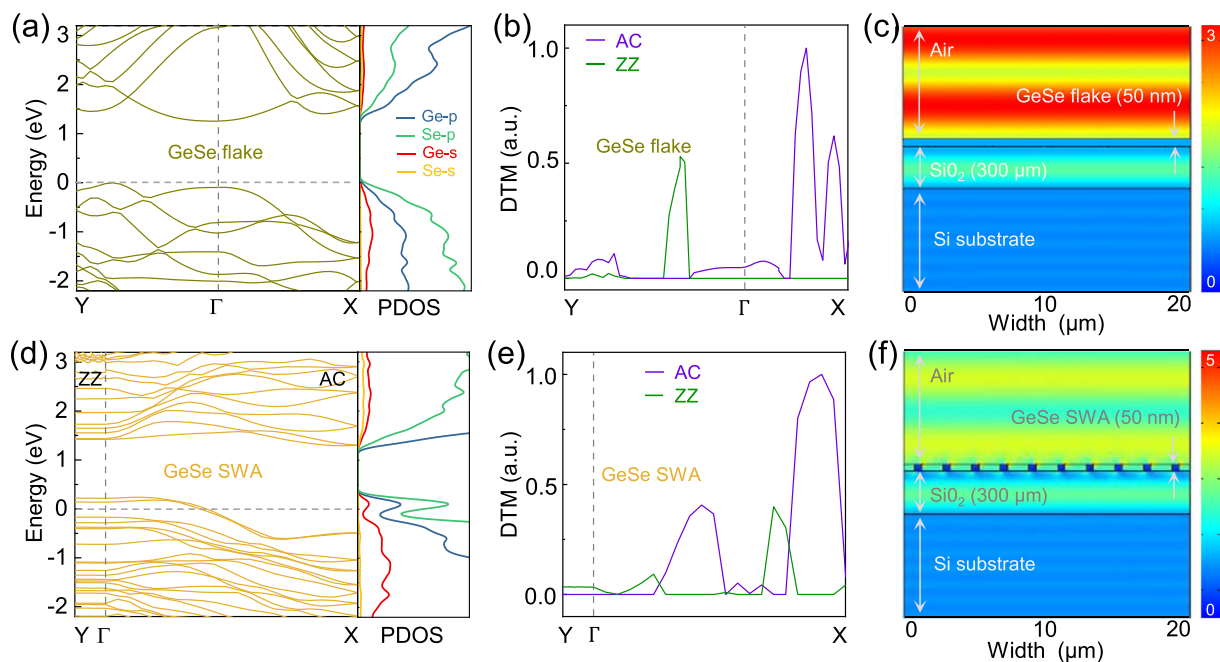


Fig. 4. Mechanism of the increased anisotropic sensitivity of GeSe SWA. Band structure of the GeSe flake (a) and GeSe SWA (d) with an indirect bandgap of 1.3 eV. The quantum confinement effect occurs along the zigzag direction of GeSe SWA (from Γ to Y). The DTM along the armchair (from Γ to X) and zigzag direction of GeSe flake (b) and GeSe SWA (e), which reveals the restricted transition probabilities of incident light along the zigzag directions. Simulated light electric field distribution of the GeSe flake mode (c) and GeSe SWA mode (f) at 800 nm, which display the surface plasmon trapping in SWA pattern.

ity of photoelectrons within the band edge can be described by the dipole transition matrixes (DTM) derived from formula of $\langle \varphi_{CBM} | \nabla_y | \varphi_{VBM} \rangle$ and $\langle \varphi_{CBM} | \nabla_x | \varphi_{VBM} \rangle$, where $\varphi_{CBM}/\varphi_{VBM}$ denotes the wave function of conduction band minimum/value based management and ∇_x, ∇_y are the momentum operators

along x and y direction. As shown in Fig. 4e, after the SWA patterning, the DTM elements of GeSe along the zigzag direction disappeared, and the transition probability ratio (P_{AC}/P_{ZZ}) was significantly enhanced correspondingly, which accounts for the high PR value of GeSe SWA. Meanwhile, the simulation of the light

electric field distributes shows the reflection off from the GeSe flake (Fig. 4f) and the localized surface plasma in the surface of GeSe SWA (Fig. 4f), enhancing the light trapping in GeSe SWA. Both the increased optical adsorption and restricted transition probability contribute to the polarization ratio enhancement of the sub-wavelength array significantly.

It is worth noting that the GeSe SWA pattern has not introduced any impurity levels in the band structure and the partial density of states (PDOS), making the array structure quite stable in electronic states. The self-passivation effect of charge density in the array boundary also demonstrates its stability after the patterning process (Fig. S12 online), which determines the defect doping could not influence the degree of polarization ratio.

4. Conclusion

In conclusion, we designed a GeSe-based SWA photodetector, which can enhance the polarization ratios and improve the broad-spectrum photodetection performance simultaneously. This result benefits from the improvement of photo absorption efficiency in the armchair direction and the restriction of transition probability along the zigzag direction. The photodetection based on GeSe SWA at the condition of BN package is the potential candidate of the commercial detector for compatible fabrication process with commercial CMOS. The strategy of constructing the low symmetric model is applicable to other in-plane anisotropic low-dimensional materials and is expected to further improve the anisotropy of linearly polarized photodetectors of them, which will greatly benefit the development of remote sensing, visual imaging, and navigation.

Conflict of interest

The authors declare that they have no conflict of interest.

Acknowledgments

This work was supported by the National Natural Science Foundation of China (62125404, 62004193, 61922077, 12274456, 92163206, 51991342, and 11874347), the Strategic Priority Research Program of Chinese Academy of Sciences (XDB43000000), the Guangdong Major Project of Basic and Applied Basic Research (2021B0301030002), and the National Key R&D Program of China (2021YFA1400502 and 2022YFA1405600). H.-X. D. was also supported by the Youth Innovation Promotion Association of Chinese Academy of Sciences (Y2021042). Z.Z. acknowledge the Nanofabrication Laboratory in the National Centre for Nanoscience and Technology for the electron beam lithography.

Author contributions

Zhongming Wei, Hui-Xiong Deng, and Can Liu supervise the project. Ziqi Zhou conducted the sample growth, device fabrication and measurement. Tao Shen, Pan Wang, Yue-Yang Liu, and Hui-Xiong Deng performed the theoretical calculations. Quanlin Guo performed the STEM experiments. Kaiyao Xin, Kai Zhao, Yali Yu, and Biao Qin helped sample characterizations. Hao Hong and Qinghe Wang helped analysis SHG spectrum date. Chenjun Ma helped the calculation in COMSOL Multiphysics software. Kaihui Liu and Juehan Yang helped analysis photoelectrical date. Ziqi Zhou, Can Liu, and Kaihui Liu wrote the article. Hui-Xiong Deng and Zhongming Wei revised the manuscript. All the authors discussed the results and commented on the manuscript.

Appendix A. Supplementary materials

Supplementary materials to this article can be found online at <https://doi.org/10.1016/j.scib.2023.01.013>.

References

- [1] Jin M, Lu F, Belkin MA. High-sensitivity infrared vibrational nanospectroscopy in water. *Light Sci Appl* 2017;6:e17096.
- [2] Rubin NA, D'Aversa G, Chevalier P, et al. Matrix Fourier optics enables a compact full-Stokes polarization camera. *Science* 2019;365:43.
- [3] Zhang Z, Wang S, Liu C, et al. All-in-one two-dimensional retinomorph hardware device for motion detection and recognition. *Nat Nanotechnol* 2022;17:27–32.
- [4] Lepetit T, Kanté B. Simultaneous Stokes parameters. *Nat Photonics* 2015;9:709–10.
- [5] Macchi A, Pegoraro F. Global position by polarization. *Nat Photonics* 2018;12:314–5.
- [6] Martínez A. Polarimetry enabled by nanophotonics. *Science* 2018;362:750–1.
- [7] Li Q, Groep J, Wang Y, et al. Transparent multispectral photodetectors mimicking the human visual system. *Nat Commun* 2019;10:4982.
- [8] Kogos LC, Li Y, Liu J, et al. Plasmonic ommatidia for lensless compound-eye vision. *Nat Commun* 2020;11:1637.
- [9] Tong L, Peng Z, Lin R, et al. 2D materials-based homogeneous transistor-memory architecture for neuromorphic hardware. *Science* 2021;373:1353–8.
- [10] Empedocles SA, Neuhauser R, Bawendi MG. Three-dimensional orientation measurements of symmetric single chromophores using polarization microscopy. *Nature* 1999;399:126–30.
- [11] Tyo J, Dennis L, David B, et al. Review of passive imaging polarimetry for remote sensing applications. *Appl Opt* 2006;45:5453–69.
- [12] Lin KT, Chen HL, Lai YS, et al. Silicon-based broadband antenna for high responsivity and polarization-insensitive photodetection at telecommunication wavelengths. *Nat Commun* 2014;5:3288.
- [13] Maruyama Y, Terada T, Yamazaki T, et al. 3.2-MP back-illuminated polarization image sensor with four-directional air-gap wire grid and 2.5- μm pixels. *IEEE Trans Electron Devices* 2018;65:2544–51.
- [14] Wei J, Xu C, Dong B, et al. Mid-infrared semimetal polarization detectors with configurable polarity transition. *Nat Photonics* 2021;15:614–21.
- [15] Fan T, Xie Z, Huang W, et al. Two-dimensional non-layered selenium nanoflakes: facile fabrications and applications for self-powered photodetector. *Nanotechnology* 2019;30:114002.
- [16] Qiao H, Huang Z, Ren X, et al. Self-powered photodetectors based on 2D materials. *Adv Opt Mater* 2020;8:1900765.
- [17] Zhang Y, Huang P, Guo J, et al. Graphdiyne-based flexible photodetectors with high responsivity and detectivity. *Adv Mater* 2020;32:2001082.
- [18] Gao L, Ma C, Wei S, et al. Applications of few-layer Nb₂C MXene: narrow-band photodetectors and femtosecond mode-locked fiber lasers. *ACS Nano* 2021;15:954–65.
- [19] Xia F, Wang H, Xiao D, et al. Two-dimensional material nanophotonics. *Nat Photonics* 2014;8:899–907.
- [20] Liu S, Xiao W, Zhong M, et al. Highly polarization sensitive photodetectors based on quasi-1D titanium trisulfide (TiS₃). *Nanotechnology* 2018;29:184002.
- [21] Liu C, Xu X, Qiu L, et al. Kinetic modulation of graphene growth by fluorine through spatially confined decomposition of metal fluorides. *Nat Chem* 2019;11:730–6.
- [22] Cui Y, Zhou Z, Li T, et al. Versatile crystal structures and (opto)electronic applications of the 2D metal mono-, di-, and tri-chalcogenide nanosheets. *Adv Funct Mater* 2019;29:1900040.
- [23] Zhang Q, Hu G, Ma W, et al. Interface nano-optics with van der Waals polaritons. *Nature* 2021;597:187–95.
- [24] Yu Y, Xiong T, Zhao K, et al. Tunable alloying improved wide spectrum UV-Vis-NIR and polarization-sensitive photodetector based on Sb–S–Se nanowires. *IEEE Trans Electron Devices* 2021;68:3887–93.
- [25] Wang J, Xu X, Cheng T, et al. Dual-coupling-guided epitaxial growth of wafer-scale single-crystal WS₂ monolayer on vicinal a-plane sapphire. *Nat Nanotechnol* 2022;17:33–8.
- [26] Wang Y, Gu Y, Cui A, et al. Fast uncooled mid-wavelength infrared photodetectors with heterostructures of van der Waals on epitaxial HgCdTe. *Adv Mater* 2022;34:2107772.
- [27] Zhang Q, Qingdong O, Guangwei H, et al. Unidirectionally excited phonon polaritons in high-symmetry orthorhombic crystals. *Sci Adv* 2022;8:eabn9774.
- [28] Wang X, Xiong T, Zhao K, et al. Polarimetric image sensor and Fermi level shifting induced multichannel transition based on 2D PdPS. *Adv Mater* 2022;34:2107206.
- [29] Zhao K, Yang J, Zhong M, et al. Direct polarimetric image sensor and wide spectral response based on quasi-1D Sb₂S₃ nanowire. *Adv Funct Mater* 2020;31:2006601.
- [30] Guo Z, Cao R, Wang H, et al. High-performance polarization-sensitive photodetectors on two-dimensional $\beta\text{-InSe}$. *Natl Sci Rev* 2022;9:nwab098.
- [31] Xia F, Wang H, Jia Y. Rediscovering black phosphorus as an anisotropic layered material for optoelectronics and electronics. *Nat Commun* 2014;5:4458.

- [32] Wang X, Jones AM, Seyler KL, et al. Highly anisotropic and robust excitons in monolayer black phosphorus. *Nat Nanotechnol* 2015;10:517–21.
- [33] Deng B, Tran V, Xie Y, et al. Efficient electrical control of thin-film black phosphorus bandgap. *Nat Commun* 2017;8:14474.
- [34] Xia F, Wang H, Hwang JCM, et al. Black phosphorus and its isoelectronic materials. *Nat Rev Phys* 2019;1:306–17.
- [35] Tan D, Lim HE, Wang F, et al. Anisotropic optical and electronic properties of two-dimensional layered germanium sulfide. *Nano Res* 2016;10:546–55.
- [36] Long M, Gao A, Wang P, et al. Room temperature high-detectivity mid-infrared photodetectors based on black arsenic phosphorus. *Sci Adv* 2017;3:e1700589.
- [37] Chen Y, Chen C, Kealhofer R, et al. Black arsenic: a layered semiconductor with extreme in-plane anisotropy. *Adv Mater* 2018;30:e1800754.
- [38] Zhou Z, Long M, Pan L, et al. Perpendicular optical reversal of the linear dichroism and polarized photodetection in 2D GeAs. *ACS Nano* 2018;12:12416–23.
- [39] Zhong M, Meng H, Liu S, et al. In-plane optical and electrical anisotropy of 2D black arsenic. *ACS Nano* 2021;15:1701–9.
- [40] Cui Y, Zhou Z, Wang X, et al. Wavelength-selectivity polarization dependence of optical absorption and photoresponse in SnS nanosheets. *Nano Res* 2021;14:2224–30.
- [41] Yan Y, Xiong W, Li S, et al. Direct wide bandgap 2D GeSe₂ monolayer toward anisotropic UV photodetection. *Adv Opt Mater* 2019;7:1900622.
- [42] Yang Y, Liu S-C, Wang X, et al. Polarization-sensitive ultraviolet photodetection of anisotropic 2D GeSe₂. *Adv Funct Mater* 2019;28:1900411.
- [43] Wang H, Qian X. Giant optical second harmonic generation in two-dimensional multiferroics. *Nano Lett* 2017;17:5027–34.
- [44] Wang X, Li Y, Huang L, et al. Short-wave near-infrared linear dichroism of two-dimensional germanium selenide. *J Am Chem Soc* 2017;139:14976–82.
- [45] Wang X, Zhong F, Kang J, et al. Polarizer-free polarimetric image sensor through anisotropic two-dimensional GeSe. *Sci China Mater* 2020;64:1230–7.
- [46] Gruev V, York T. High resolution CCD polarization imaging sensor. *Opt Express* 2010;18:19087–94.
- [47] Zhou X, Hu X, Jin B, et al. Highly anisotropic GeSe nanosheets for phototransistors with ultrahigh photoresponsivity. *Adv Sci* 2018;5:1800478.
- [48] Yuan H, Liu X, Afshinmanesh F, et al. Polarization-sensitive broadband photodetector using a black phosphorus vertical p-n junction. *Nat Nanotechnol* 2015;10:707–13.
- [49] Bullock J, Amani M, Cho J, et al. Polarization-resolved black phosphorus/molybdenum disulfide mid-wave infrared photodiodes with high detectivity at room temperature. *Nat Photonics* 2018;12:601–7.
- [50] Huo N, Yang J, Huang L, et al. Tunable polarity behavior and self-driven photoswitching in p-WSe₂/n-WS₂ heterojunctions. *Small* 2015;11:5430–8.
- [51] Jia R, Zhao D, Gao N, et al. Polarization enhanced charge transfer: dual-band GaN-based plasmonic photodetector. *Sci Rep* 2017;7:40483.
- [52] Ran W, Ren Z, Wang P, et al. Integrated polarization-sensitive amplification system for digital information transmission. *Nat Commun* 2021;12:6476.
- [53] Zuo Y, Yu W, Liu C, et al. Optical fibres with embedded two-dimensional materials for ultrahigh nonlinearity. *Nat Nanotechnol* 2020;15:987–91.
- [54] Jia W, Fu J, Cao Z, et al. Fast plane wave density functional theory molecular dynamics calculations on multi-GPU machines. *J Chem Phys* 2013;251:102–15.
- [55] Jia W, Cao Z, Wang L, et al. The analysis of a plane wave pseudopotential density functional theory code on a GPU machine. *Comput Phys Commun* 2013;184:9–18.
- [56] Kohn W, Sham LJ. Self-consistent equations including exchange and correlation effects. *Phys Rev* 1965;140:A1133–8.
- [57] Heyd J, Scuseria GE, Ernzerhof M. Hybrid functionals based on a screened Coulomb potential. *J Chem Phys* 2003;118:8207–15.
- [58] Hamann DR. Optimized norm-conserving vanderbilt pseudopotentials. *Phys Rev B* 2013;88:085117.



Ziqi Zhou received her B.S. degree from Lanzhou University in 2015, and Ph.D. degree from Institute of Semiconductors, Chinese Academy of Sciences in 2021. Currently, she is working as a postdoctoral fellow at Peking University. Her research interest includes the growth, electric engineering, and optoelectronics of low-dimensional semiconductors.



Can Liu received her B.S. degree from Northwestern Polytechnical University in 2014, and Ph.D. degree from Peking University in 2019. From 2019 to 2022, she worked as a postdoctoral fellow at Peking University. Currently, she is a principle investigator at Renmin University of China. Her research interest includes the interfacial modulation growth of single-crystal 2D materials and their optical characterizations.



Hui-Xiong Deng received his B.S. degree from Inner Mongolia University in 2005, and Ph.D. degree from Institute of Semiconductors, Chinese Academy of Sciences in 2010. From 2011 to 2014, he worked as a postdoctoral fellow at National Renewable Energy Laboratory (NREL), USA. Currently, he is a professor at the Institute of Semiconductors, Chinese Academy of Sciences. His research interest includes semiconductor physics, doping and defect physics in semiconductors, calculations and design of properties of optoelectronic and microelectronic materials.



Zhongming Wei received his B.S. degree from Wuhan University in 2005, and Ph.D. degree from Institute of Chemistry, Chinese Academy of Sciences in 2010. From 2010 to 2015, he worked as a postdoctoral fellow and then assistant professor at University of Copenhagen, Denmark. Currently, he is working as a professor at Institute of Semiconductors, Chinese Academy of Sciences. His research interest includes low-dimensional semiconductors and their optoelectronic devices.